Proceedings of the 2006 IEEE/RSJ
International Conference on Intelligent Robots and Systems
October 9 - 15, 2006, Beijing, China

# Power Electronics Design Choice for Piezoelectric Microrobots

E. Steltz, M. Seeman, S. Avadhanula, and R.S. Fearing
*Department of EECS, University of California, Berkeley, CA 94720*

{*ees132 mseeman srinath ronf*} *@eecs.berkeley.edu*

***Abstract*— Piezoelectric actuators are advantageous for microrobots due to their light weight, high bandwidth, high force production, low power consumption, and simplicity of integration. However, the main disadvantage of either stack or cantilever piezoelectric actuators are the high drive voltages required for adequate force and displacement. This especially limits the ability for such actuators to be used in autonomous microrobots because of the weight and complexity of necessary power electronics. This paper approaches the design of all the component parts of an autonomous piezoelectric robot as a linear constraint on the weight and efficiency of those components. It then focuses on the choice and optimization of the power electronics section of the robot, specifically exploring three different high voltage generation methods. Finally, one of these power electronics designs is implemented and its behavior is experimentally explored.**

***Index Terms*— piezoelectric, high voltage, charge pump, autonomous, microrobots**

## I. Introduction

Piezoelectric actuators, both stack and cantilever type, have become increasingly popular for driving microrobots (here defined as centimeter scale, 10g or less robots). In our lab in particular, piezoelectric bending actuators such as those in [1] have been used for the steering surface actuation for a small microglider [2], the motors for a flapping micro air vehicle called the MFI (Micromechanical Flying Insect) [3], and actuators for a small crawling robot [4]. These actuators have high bandwidth, high force output, and very low weight due to their ability to scale down. The main disadvantage of piezoelectric actuators has been the high voltage required to obtain significant force or displacement from them. This is less of the case in piezoelectric stack actuators, where small displacements are expected and 50 V is a satisfactory driving voltage. In fact, autonomous microrobots utilizing piezoelectric stack actuators have been created by Montane et al. [5] using an operational amplifier based driving scheme for the MICRON robot [6]. However, for the large displacement dynamic movement aimed for here, stack actuators are not interesting.

In bending actuators, however, voltages up to around 300 V are sometimes necessary, corresponding to several hundred $\mu$m of actuator displacement and many mN of force output (it should be noted that this high voltage can be avoided as shown in [7] but it is nontrivial to construct such actuators). Generating this high voltage while still maintaining design requirements has proven challenging, and therefore autonomous piezoelectric robots utilizing cantilever actuators are few in number. For systems such as small crawling robots or tiny fliers (such as the microglider), the need for a lightweight high voltage power supply is necessary.

This paper explores the broad design problem of an autonomous piezoelectric robot, constraining it to using existing cantilever actuator technology, off the shelf battery technology, and carbon fiber flexures and links for transmissive elements as in [3]. The design space is thus the sizing of these component technologies plus the design of the robot's power electronics, for which several different methods will be considered for high voltage generation. This analysis culminates in the construction of a fully operational high voltage amplifier and drive scheme capable of driving a variety of microrobots.

## II. Autonomous Microrobot Constraints

For a robot less than 10g, much of the challenge is sizing all components properly so that the robot has the necessary power density to dynamically move itself around its environment. This is governed by the robot's battery technology, actuators, transmissive and structural elements, and power electronics. The component parts of such a robot are shown in block diagram form in Fig. 1 along with the efficiencies ($\eta_x$) and power outputs for each stage ($P_x$). The total mass of the robot is given by

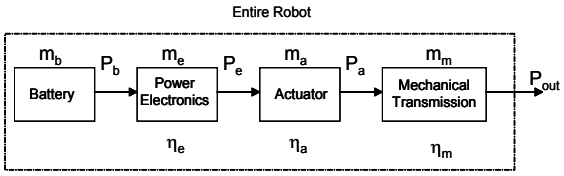


Fig. 1. Block diagram of autonomous microrobot

$$m_b + m_e + m_a + m_m = M_{Robot} \tag{1}$$

where the masses are those of the battery, power electronics, actuators, and mechanical transmissive elements $m_m$, which is also assumed to include the weight of all structural support elements of the robot. The power output of each stage as shown in Fig. 1 can be related to the power densities $\gamma$ of each stage by

$$P_x = m_x \gamma_x \tag{2}$$

where x denotes the component of the robot. The total efficiency of the robot is denoted

$$P_{out} = \eta_e \eta_a \eta_m P_{batt} \tag{3}$$

Starting from Equation 1 and substituting the relations to the power densities given by 2, one obtains

$$\frac{P_{batt}}{\gamma_b} + \frac{P_e}{\gamma_e} + \frac{P_a}{\gamma_a} + \frac{P_{out}}{\gamma_m} = \frac{P_{out}}{\gamma_{robot}} \tag{4}$$

Finally, the efficiency relation in Eq. 3 can be applied to find

$$\frac{1}{\eta_e \eta_a \eta_m \gamma_b} + \frac{1}{\eta_a \eta_m \gamma_e} + \frac{1}{\eta_m \gamma_a} + \frac{1}{\gamma_m} = \frac{1}{\gamma_{robot}} \tag{5}$$

An estimate of the power density for the robot to be designed is now necessary. Power density for a statically stable robot can be quite low; however, robots with dynamic abilities are of interest here. One very simple method of determining an interesting power density number is to consider a rope climbing robot climbing a vertical rope at a rate $v$. Then the power density of the robot is simply $gv$, which for reasonable climbing speeds for a high performance microrobot might be in the range of 50 to 100 cm/s, yielding power densities of 5 to 10 W/kg. This analysis assumes that all power output of the robot goes directly to its potential energy with no power losses. We could also use the example of a crawling/walking robot and the idea of specific resistance. If we use the value of 1.2 for specific resistance of a crawler as given in [8], a 2g robot moving at 0.5 m/s would have a power density of 5.5 W/kg.

Looking further into this question of reasonable power density values, one can look to animals on the scale we are interested in, for instance fruitflies (e.g. *Drosophila virilis*), dragonflies (*Aeschna juncea*), or moths (*Manduca sexta*), although flapping flight is a very high performance metric and the power densities of these animals is probably too high for our design purposes. For a more reasonable performance number, the cockroaches *Periplaneta americana* or *Blaberus discoidalis* could be of interest. The estimated power densities for these insects appear in Table I. For all flying insects, the power density is that for hovering; the total power density of the animal is most likely higher since the insects can do more advanced aerial maneuvers. All power density numbers are also the computed or measured power output to the environment; the actual power expended by the animal to impart this usable power to the environment would be higher. Data in Table Itaken from [9],[10],[11], [12], [13], and [14]

Considering that the microrobot we are designing probably does not need to be as agile as a flapping insect in hover but might want to be as powerful as the fast cockroach *Periplaneta americana*, we will aim at a power density of 10 W/kg for our microrobots, which is also in the range of the simple climbing robot estimation from earlier and the estimate using the specific resistance of a crawler. This value will be treated as a known value for $\gamma_{robot}$ on the right side of Eq. 5.

| Insect | Mass(g) | $P_{env}$(mW) | $\gamma_{env}$(W/kg) |
|---|---|---|---|
| Drosophila virilis | 0.001 | .03 | 30 |
| Aeschna juncea | 0.8 | 29.6 | 37 |
| Periplaneta americana | 0.8 | 1 | 1.25 |
| Manduca sexta | 2.0 | 36 | 18 |
| Blaberus discoidalis | 2.6 | 0.83 | 0.32 |

TABLE I

TYPICAL POWER DENSITIES FOR VARIOUS FLYING AND CRAWLING INSECTS.

## III. DETERMINATION OF POWER DENSITIES AND EFFICIENCIES

This section describes the experimental setup and methodology to determine the power density and efficiency numbers mentioned in the previous section.

### A. Actuator Power Density and Efficiency

To determine the actuator parameters $\eta_a$ and $\gamma_a$, the actuator is connected to a single degree of freedom (1 DOF) fourbar connected so that it can flap a wing from the MFI project, about 10 mm in length. A diagram of the setup appears in Fig. 2. The advantage of using such a setup to determine actuator efficiency is that the mechanical power output of the fourbar/wing will be dominated by aerodynamic forces, and the aerodynamic power output can be easily modeled and calculated as follows. The fourbar

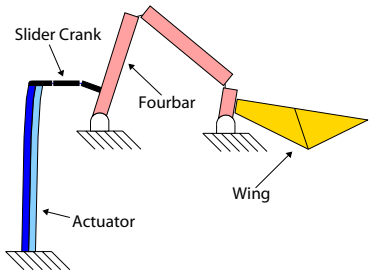


Fig. 2. Actuator/fourbar/wing test setup. Figure taken from [3]

can be regarded as a mechanical amplifier which converts the small actuator motion ($\approx$ 500 microns) into a rotary motion of the wing ($\pm 50°$). The whole system can be modeled as

$$J\ddot{\theta} + B_1\dot{\theta} + B_2\dot{\theta}|\dot{\theta}| + k_0\theta(1 - a\theta^2) = T_i(\theta)V \tag{6}$$

where $J$ is the effective inertia in the wing coordinate system, $B_1$ is the linear damping coefficient (which arises mostly from losses in the transmission mechanism) and $B_2$ is the viscous damping coefficient, which arises mostly from the wing aerodynamics (with a small contribution from the structural losses). $V$ is the input voltage applied to the actuator and $T_i$ is the constant which relates the applied input voltage to the torque generated at the wing hinge. Certain actuator nonlinearities, including hysteresis, creep, and possibly force dependent damping, are neglected in the model for simplicity. Typically for the fourbar mechanism

used in the MFI, we have $J = 22 \times 10^{-12} kgm^2$, $B_1 = 2.6 \times 10^{-9} Nms/rad$, $B_2 = 8.6 \times 10^{-12} Nms^2/rad^2$, $k_0 = 4.5 \times 10^{-5} Nm/rad$. These parameters were extracted by performing a frequency domain system identification of the model above.

We apply a known input voltage $V(t) = V_{DC} + V_0 \sin \omega t$ to the actuator and measure the output waveform $\theta(t)$ and the current going into the actuator $I(t)$. Since the system is nonlinear $\theta(t)$ and $I(t)$ are not sinusoidal, but for the range of motions we are interested in, the higher harmonics are negligible. The power delivered to the structure is measured as:

$$P_{out} = \frac{1}{T} \int_0^T (B_1 \dot{\theta} + B_2 \dot{\theta} |\dot{\theta}|) \dot{\theta} dt \tag{7}$$

where $T = 2\pi/w$, the wing beat period. This becomes

$$P_{out} = \frac{1}{2} (B_1 + B_2 \frac{8}{3\pi} \theta_0 \omega) \theta_0^2 \omega^2 \tag{8}$$

where $\omega$ is the frequency (in $rads/s$) of the applied input voltage and $\theta_0$ is the amplitude of the first harmonic of the measured output angle of the wing.

In calculating the electrical power delivered to the actuator, we must consider that charge recovery methods (such as those mentioned in [15] may need to be applied to recover the energy stored in the actuator capacitance when it is charged. First we will consider the case with no charge recovery. In this case, we integrate $I(t)V(t)$ over the part of the cycle for which the product $I(t)V(t)$ is positive (in other words, we are calculating true power, not apparent power which would include the power returned from our actuator capacitance). Assuming that $V(t)$ is always positive (because of the added DC offset) and that $I(t) = I_0 \sin(\omega t + \phi_i)$, this becomes:

$$\begin{aligned} P_{in} &= \int_{-\phi_i/\omega}^{(\pi-\phi_i)/\omega} I(t)V(t)dt \\ &= \frac{1}{4} I_0 V_0 \cos \phi_i + \frac{1}{\pi} I_0 V_{DC} \end{aligned} \tag{9}$$

With charge recovery, we reacquire part of the energy during the part of the cycle for which $I(t)V(t) < 0$. Thus with a charge recovery scheme where we reclaim $\eta_{CR}$ fraction of the energy, we have

$$\begin{aligned} P_{in} &= \int_{-\phi_i/\omega}^{(\pi-\phi_i)/\omega} I(t)V(t)dt \\ &\quad + \eta_{CR} \int_{(\pi-\phi_i)/\omega}^{(2\pi-\phi_i)/\omega} I(t)V(t)dt \\ &= \frac{1}{4} I_0 V_0 \cos \phi_i (1 + \eta_{CR}) + \frac{1}{\pi} I_0 V_{DC} (1 - \eta_{CR}) \end{aligned} \tag{10}$$

The electro-mechanical efficiency of the actuator is then given by:

$$\eta_a = \frac{P_{out}}{P_{in}}$$

Applying this to the experimentally measured data shown in Fig. 3, we get $\eta_a$ as a function of frequency as shown in Fig. 4(a). As is expected, the efficiency of the actuator is high in a narrow band around the resonance of the structure. This implies that a robot based on such actuators needs to be driven at resonance to operate at acceptable actuator efficiency. The implementation of charge recovery will be considered as part of the efficiency of the actuator, $\eta_a$; the dependence of the two is shown in Fig. 4. With zero charge recovery, we get an efficiency of about 8% and for perfect charge recovery, this increases to about 35% (again, at resonance).

In comparison, it is difficult to scale down electromagnetic motors as much as piezoelectric actuators, but there do exist motors around 0.1g with 26.5% maximum efficiency (Smoovy series 0206). However, these motors require a gearhead to reduce their high rpm, if we assume this is 50% efficient, total efficiency is only around 13%. When one allows motor mass to be higher (around 6-10g), however, motor efficiencies are commonly around 75-80% [16] and thus outperform piezoelectric actuators at this scale.

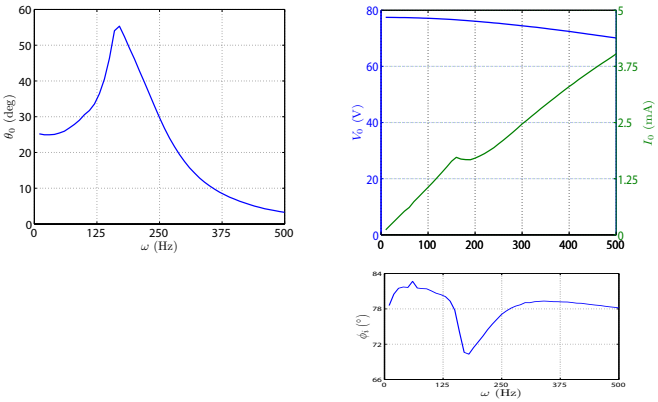


Fig. 3. Experimentally measured data showing $\theta_0$, $V_0$, $I_0$ and $\phi_i$ vs. $\omega$.

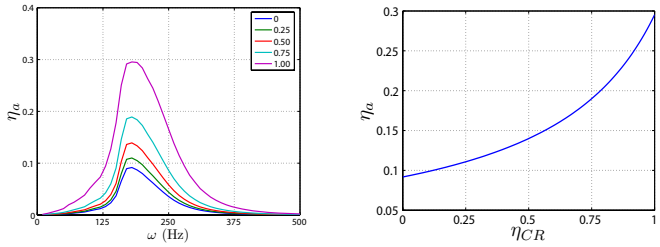


(a) $\eta_a$ vs. $\omega$ for various $\eta_{CR}$ (b) $\eta_{a,max}$ vs. $\eta_{CR}$

Fig. 4. Actuator efficiency

Power density of our piezoelectric actuator can readily be calculated knowing that a 130 mg piezoelectric actuator can drive our fourbar/wing setup through 120 degrees of flapping at 180 Hz, which yields an aerodynamic power output around 20 mW. This gives a power density value of $\gamma_a$ =160 W/kg. The actuator was known to be oversized for this application, so the maximum power density is probably higher than this value. However, since not all scaling effects of piezoelectric actuators are known (up or down), this conservative value will be used for the power density of the actuator for future calculations.

### B. Structural Power Density and Efficiency

In this section, we will analyze the power density and efficiencies of the structures described in [3]. These structures are made from carbon fiber (CF) rigid links with kapton flexures acting as rotary joints. Since they are made of CF, these structures are naturally light and strong. We consider the MFI as a representative example for calculating the power density and efficiencies which can be achieved in other robots at this scale. For the MFI, the total mechanical components weigh about 30mg. Considering that we can deliver about 60mW to the air through this structure, we get a power density of 2kW/kg.

To estimate the efficiency, we need to estimate the total internal damping in the structure. Once again we consider the 1 DOF structure described in the previous section as a representative example. To find the total internal damping in the structure, we perform frequency domain identification on the structure in (partial) vacuum and extrapolate to find $B_1$ and $B_2$ in the absence of any air. This gives us an estimate of the total internal damping in the structure. For the fourbar structure described previously, we get $B_1 = 1.3 \times 10^{-9} Nms/rad$ and $B_2 = 8.3 \times 10^{-13} Nms^2/rad^2$. Thus in our partial vacuum, $B_1$ drops by half while $B_2$ drops by an order of magnitude. This is expected since the major contributor to $B_2$ (in air) is the wing aerodynamic force. Using this $B_1$ and $B_2$, we get the power dissipated in the structure to be about 2mW for 20mW total input power. This gives an efficiency of about 90% for the fourbar structure.

Thus for the structural components, we will use

| | |
|---|---|
| $\eta_m$ | 90% |
| $\gamma_m$ | 2kW/kg |

Finally, off the shelf batteries will be used for practicality. Current state of the art lightweight batteries have lithium polymer chemistry with tremendous power densities. The power density and weights for several Kokam batteries readily available from http://www.roomflight.com are plotted in Fig. 5, all discharged at 5C (i.e. each battery will last 12 minutes). As one can see, power density at this discharge rate has a maximum of around 700 W/kg for the chemistry, but because of a higher percentage of packaging to energy storage material, power density falls to around 450 W/kg for the lightest 0.81g battery. There are many other batteries of similar power density and weight available, but for simplicity, we will assume a battery of arbitrary weight but power density along the curve of Fig. 5 is available. This will give us $\gamma_b$ in Eq. 5.

## IV. Example Calculations for 3 Different Robot Sizes

Three different robots will now be proposed with the framework formed. The masses of these robots will be 2,4, and 10g respectively, and using a power density of 10W/kg, the final output power of the robots will be $P_{out} = 20mW$, $P_{out} = 40mW$, and $P_{out} = 100mW$. This imposes the obvious constraint that the maximum power output of the

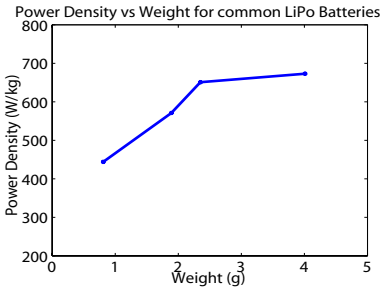


Fig. 5. Power densities for lightweight lithium polymer batteries discharged at 5C

power electronics $P_e$ must satisfy

$$P_e >= \frac{P_{out}}{\eta_a \eta_m} \tag{11}$$

A more interesting constraint appears when we substitute the known efficiencies and power densities given above into Eq. 5, yielding

$$\frac{C_1}{\eta_e} + \frac{C_2}{\gamma_e} <= C_3 \tag{12}$$

where C1, C2, and C3 are constants (with appropriate units). If one wishes to express the constraint explicitly in terms of the mass of the power electronics rather than the power density, we have

$$\frac{K_1}{\eta_e} + m_e <= K_2 \tag{13}$$

again for K1 and K2 constants with their associated units, all calculated from known power densities, masses, and efficiencies. From this equation, one can see that efficiency and mass are not necessarily of the same importance. If the ratio $K1/m$, where m is a nominal mass of an electronics design, is above 1, then efficiency is actually more important and an improvement in efficiency would help the constraint be satisfied more than an equal improvement in mass would.

For the three different robots we are designing, the values for $K_1$ and $K_2$ of Eq. 13 are given in Table IV. If the efficiency and the mass of the power electronics satisfy this constraint, then the robot will exceed the required power density.

| $M_{robot}$ (g) | $P_{elec}$(mW) | $K_1$(mg) | $K_2$(mg) |
|---|---|---|---|
| 2 | 222 | 626 | 1851 |
| 4 | 444 | 1251 | 3702 |
| 10 | 1110 | 3128 | 9256 |

TABLE II

K1 and K2 in Eq. 13 for three differently sized microrobots, also showing the electrical power output necessary for the robots

These constraints will now allow us to further explore design of the high voltage generation and drive electronics portion of the robot.

## V. High Voltage Drive Technology and Analysis

There are many DC-DC converter technologies to amplify the low voltage of a battery up to higher voltages. In our case, when very high output voltages are necessary and weight and efficiency are important design variables, the design problem becomes difficult. Three main technologies will be presented here to achieve this high voltage generation: a boost converter, a transformer, and a hybrid design utilizing a boost converter along with a switched capacitor circuit. In all designs, it will be assumed that an output voltage of 250 V is desired.

### A. Boost Converter

A traditional boost converter consists of an inductor, a switching transistor, a diode, and an output capacitor, as shown in Fig. 6. The voltage of the input DC source is boosted by rapidly switching the current through the inductor and then allowing the higher voltage across the inductor to charge the capacitor.

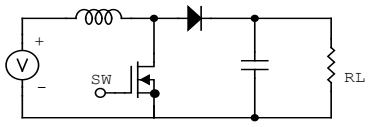


Fig. 6. Traditional boost converter topology

However, high voltage gains and output powers are difficult for this type of amplifier due to conduction losses in the inductor and switching losses in the transistor switch. Regardless, for the three power outputs of 222 mW, 444 mW, and 1.1 W (from Eq. 11, corresponding to the three different sample robot sizes we are designing), the best boost converter we could construct from commercially available components was calculated and analyzed in terms of the metric of Eq. 13. This appears along with the plots for other high voltage converter technologies in Fig. 9.

### B. Transformer Method

A standard wire wound ferrite core custom transformer would yield a very simple method for high voltage generation. Very light cores (from 30 mg) are readily available from a variety of sources and have favorable loss characteristics. Several transformers were designed with commercially available cores and secondary inductors, with the topology shown in Fig. 7. Their performance with respect to the constraint of Eq. 13 is plotted in Fig. 9. The main problem with this method, however, is the number of turns required on the secondary winding of the transformer. In the cases considered, the highest performance transformers plotted would require 8 turns on the primary, but over 1100 turns on the secondary. Manufacturing such a transformer manually would be impossible and likely cost prohibitive commercially.

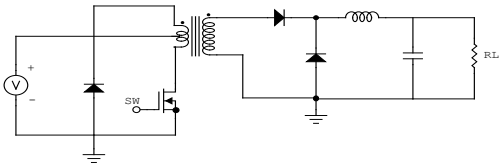


Fig. 7. Traditional forward converter topology

There are some commercially available transformer based methods that satisfy our requirements. Pico Electronics (http://www.picoelectronics.com) offers small surface mount transformers with 5V input and high voltage outputs; in this case we will consider a 250V output. The 5AV250 in particular uses a pot core transformer and a constant switching frequency and is stable with a fairly small (0.1 $\mu$F) capacitor. This commercially available technology is also plotted on Fig. 9, but the pot core alone is 2g and the packaging brings the total product up to 4g so it is only a potential technology for the heavier range of microrobots (like the 104g autonomous piezoelectric robot in [17]). Also, this transformer requires at least a 10% minimum load, which is a disadvantage if the robot is to be passive for any amount of time.

### C. Hybrid Converter

Finally, a hybrid converter using a boost converter with a cascaded charge pump circuit is considered. This method has the potential to be very light (with proper choice of small capacitors and diodes) and very efficient, for the first boost converter stage can be operated in a reasonably small voltage gain range where it can be quite efficient. The switched capacitor topology we chose is shown in Fig. 8, where Vin is the output of the boost converter, whose alternating can artificially switch the capacitors to push charge up the capacitor ladder. The performance of such a scheme is then compared in Fig. 9. The only variable in the scheme changed as more output power is demanded is the size of the capacitors in the ladder, which will go up in both value and package size for more power output.

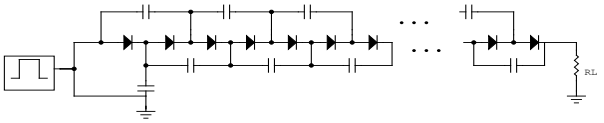


Fig. 8. Switched capacitor circuit, analyzed in cascade with a boost converter

### D. Converter Conclusion

As demonstrated in Fig. 9, a custom transformer method would be best to minimize the constraint and is therefore the most advantageous method, but as discussed earlier, the manufacturability is questionable for the device. The hybrid method is consistently better suited for our cause than the boost converter alone, and the Pico high voltage

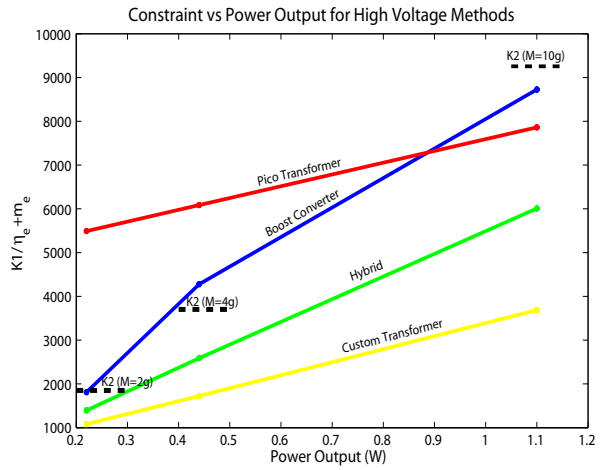


Fig. 9. Comparison of high voltage conversion methods expressed in terms of the constraint expressed earlier (all predicted).

converter can only be considered for robots that are toward the heavier region of the microrobot range but does have the advantage of being a very simple, one device solution for those robots.

## VI. Experimental Realization of Hybrid High Voltage Amplifier

Since the transformer method is not feasible, the hybrid high voltage conversion method was implemented for microrobots in the range of 2 to 4 gram. One board was created for this entire range for simplicity even though it is known that custom efficiencies and weights for individual robots would be best.

### A. First Stage - Inductor Based

A lightweight Linear Technology part, the LT1615-1, was used for the boost converter stage along with a Coilcraft 22 $\mu$H inductor (0603PS series) that weighs 28 mg. This IC has the advantage of built-in feedback and high efficiency in a lightweight (12 mg) package which minimizes not only weight but also conserves the area of the PCB that all these electronics will rest on. According to the datasheet, this part has an efficiency of around 75% at high output powers ($>$ 50 mW), but it falls to around 50% for low output powers.

### B. Second Stage - Switched Capacitor Method

The topology of Fig. 8 was used with 9 stages of capacitors/diodes to boost to 250V. The entire circuit diagram appears in Fig. 10. The average predicted efficiency of just the charge pump section is approximately 65% (though it differs with output power), and was determined with the analysis presented in [18]. This analysis also predicts a drop in efficiency of the charge pump at higher output powers; however, this drop can be mitigated by moving up a capacitor size (from 0402, 22nF capacitors to 0603, 220 nF capacitors), which both fit on the custom board.

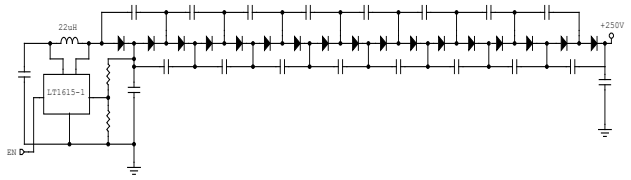


Fig. 10. Hybrid boost converter/switched capacitor circuit

Experimentally, the efficiency of the hybrid boost converter/charge pump is shown in Fig. 11 for both 22nF 0402 capacitors and 220nF 0603 capacitors. Also shown on the plot is the predicted efficiency of the hybrid voltage converter for the two cases. As one can see, the power output when using 22nF capacitors is limited (the output voltage starts drooping undesirably). However, if one moves up to 220nF capacitors, the predicted power range exceeds 200 mW. One can use this fact to increase the output of the entire circuit arbitrarily until one exceeds the power output capabilities of the boost converter.

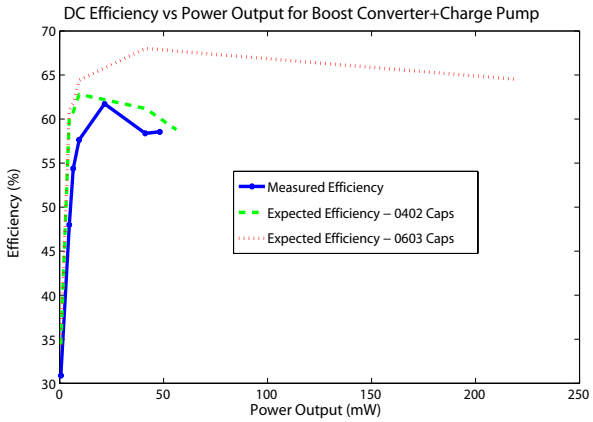


Fig. 11. DC efficiency of hybrid power supply, predicted and measured for 22nF 0402 capacitors, predicted but not verified for 0603, 220 nF capacitors

## VII. Realization of Total Design and Drive of Microrobots

The hybrid boost converter/switched capacitor method was implemented on 3 mil standard PC board and utilized 0402 capacitors and resistors for weight savings. The charge pump capacitors were 22 nF (50V maximum) and the diodes were high speed Schottky diodes, multiple diodes per package for weight saving. The actuator drive scheme shown in Fig. 12 was implemented with Supertex TN2124 NMOS transistors and FMMT558 P-type bipolar transistors along with appropriate values for the resistors based on a 10 nF actuator capacitance. For simplicity, the biasing circuitry was placed on one side of the PCB with the drive scheme on the other, as shown in Fig. 13. The populated board weighs approximately 427 mg. Of this weight, the board itself weighs 140 mg, and the drive scheme section components weigh approximately 60 mg

(for two independent actuator outputs), meaning the biasing circuitry components weigh approximately 225 mg.

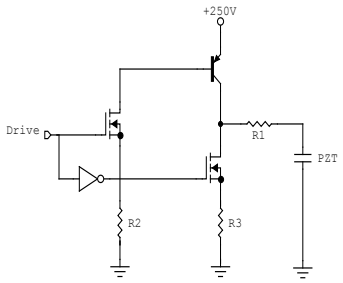


Fig. 12. Simple push-pull type high voltage piezo drive scheme

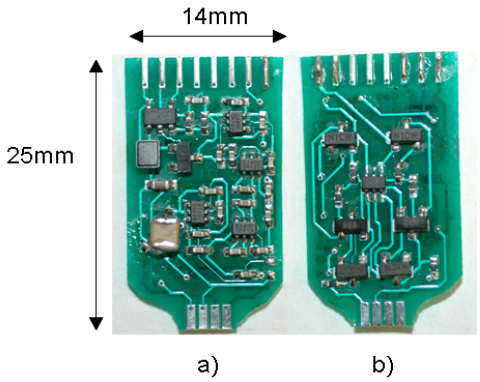


Fig. 13. 427 mg PC board with a) bias generation and b) drive realization

## VIII. Conclusion and Future Work

This paper has presented the design of high voltage power electronics for driving autonomous, piezoelectric based microrobots, in the context of the tradeoffs in the entire robot's design. Discussion of typical power densities for this scale of robot was also presented, and we found that charge recovery on the capacitance of the actuator can tremendously increase its efficiency to make piezoelectric robots more feasible (though here we have developed a series of microrobots without charge recovery, using only 10% efficient actuators).

We conclude that a hybrid voltage conversion scheme consisting of a boost converter combined with a switched capacitor circuit is the most practical technology for the power supply of microrobots, and a circuit of this type has been experimentally verified. Of particular future interest is the ability of this circuit to be implemented on a silicon chip with only one external inductor, possibly offering a 250 V power supply that weighs only 30 mg and can output several hundred milliwatts.

We have also analyzed three differently sized robots, and the associated power outputs for these robots (all incorporating hybrid converter schemes) is shown in Table VIII. Future work includes applying the power supply to a variety of microrobots, including a flapping winged flier on a tether and a variety of crawling robots.

| $M_{robot}$(g) | $P_b$(mW) | $P_e$(mW) | $P_a$(mW) | $P_{out}$(mW) |
|---|---|---|---|---|
| 2 | 363 | 222 | 22.2 | 20 |
| 4 | 693 | 444 | 44.4 | 40 |
| 10 | 1700 | 1110 | 111 | 100 |

TABLE III

Power summary for sample robots designed in this paper. Actuator efficiency is assumed to be 10%. Powers are those labeled in Fig. 1

.

## IX. Acknowledgments

The authors would like to thank Dr. Richard Groff for helpful discussions on a variety of topics and Ranjana Sahai for applying the discussed technology to a crawling robot. This work has been funded under NSF IIS-IIS-0412541.

## References

[1] R.J Wood and E. Steltz. Optimal energy density piezoelectric bending actuators. *Sensors and Actuators A*, 119/2:476–488, 2004.

[2] R.J Wood, S. Avadhanula, E. Steltz, M. Seeman, J. Entwistle, A. Bachrach, G. Barrows, S. Sanders, and R.S. Fearing. Design, fabrication and initial results of a 2g autonomous glider. In *The 31st Annual Conf. of the IEEE Indust. Elect. Soc.*, 2005.

[3] R.J. Wood, S. Avadhanula, M. Menon., and R.S. Fearing. Microrobotics using composite materials: The micromechanical flying insect thorax. In *IEEE Int. Conf. Rob. Auto.*, pages 1842–1849, Taiwan, 2003.

[4] R. Sahai, E. Steltz, S. Avadhanula, R.J. Wood, and R.S. Fearing. Towards a 3g crawling robot through the integration of microrobot technologies. In *IEEE Int. Conf. on Rob. and Auto.*, 2006.

[5] E. Montane, S.A. Bota, J. Lopez-Sanchez, P. Miribel-Catala, M. Puig-Vidal, and J. Samitier. Smart power integrated circuit for piezoceramic-based microrobot. In *ESSCIRC*, 2001.

[6] J. Brufau, M. Puig-Vidal, J. Lopez-Sanchez, and J. Samitier et. al. Micron: Small autonomous robot for cell manipulation applications. In *IEEE Int. Conf. Rob. Auto.*, pages 856–861, 2005.

[7] N. Kawahara, T. Shibata, and T. Sasaya. In-pipe wireless micro robot. In *Proceedings of SPIE*, pages 166–171, 1999.

[8] N. Neville and M. Buehler. Towards bipedal running of a six legged robot. In *12th Yale Workshop on Adapt. and Learning Sys.*, 2003.

[9] M. Sun and J. Tang. Lift and power requirements of hovering flight in drosophila virilis. *J. Exp. Biol*, 205:2413–2427, 2002.

[10] R. Ake Norberg. The pterostigma of insect wings an inertial regulator of wing pitch. *J. Comp. Physiol*, 81:9–22, 1972.

[11] R.J. Full and M.S. Tu. Mechanics of rapid running insect: Two-, four- and six-legged locomotion. *J. Exp. Biol.*, 156:215–231, 1991.

[12] R.J. Full and M.S. Tu. Mechanics of six-legged runners. *J. Exp. Biol.*, 148:129–146, 1990.

[13] R. Dudley. *The Biomechanics of Insect Flight*. Princeton University Press, 2000.

[14] M. Sun and S. Lan. A computational study of the aerodynamic forces and power requirements of dragonfly (aeschna juncea) hovering. *J. Exp. Biol.*, 207:1887–1901, 2004.

[15] D. Campolo, M. Sitti, and R.S. Fearing. Efficient charge recovery method for driving piezoelectric actuators with quasi-square waves. *IEEE Transactions on Ultrasonics, Ferroelectrics, and Frequency Control*, 50, 2003.

[16] M. Keenon and J. Grasmeyer. Development of the black widow and microbat mavs and a vision of the future of mav design. In *AIAA Int. Air and Space Symp. and Exp.: The Next 100 Years*, 2003.

[17] M. Goldfarb, M. Gogola, G. Fischer, and E. Garcia. Development of a piezoelectrically-actuated mesoscale robot quadraped. *Journal of Micromechatronics*, 1:205–219, 2002.

[18] M. Seeman and S. Sanders. Analysis and optimization of switched-capacitor dc-dc converters. In *To appear in IEEE COMPEL*, 2006.